Atmos. Chem. Phys. Discuss., 11, 14091–14125, 2011
www.atmos-chem-phys-discuss.net/11/14091/2011/
doi:10.5194/acpd-11-14091-2011

Atmospheric Chemistry and Physics Discussions

Variability of aerosol optical properties in the Western Mediterranean Basin

M. Pandolfi, M. Cusack, A. Alastuey, and X. Querol

Institute of Environmental Assessment and Water Research (IDAEA-CSIC), Barcelona, Spain

Received: 18 February 2011 – Accepted: 25 April 2011 – Published: 9 May 2011

Correspondence to: M. Pandolfi (marco.pandolfi@idaea.csic.es)

Published by Copernicus Publications on behalf of the European Geosciences Union.

Abstract

Aerosol light scattering, black carbon (BC) and particulate matter (PM) concentrations were measured at Montseny, a regional background site in the Western Mediterranean Basin (WMB) which is part of the European Supersite for Atmospheric Aerosol Research (EUSAAR). Off line analyses of 24 h PM filters collected with Hi-Vol instruments were performed for the determination of the main chemical components of PM. Measurements of BC were used to calculate the light absorption properties of atmospheric particles. Single Scattering Albedo (SSA) at 635 nm was estimated starting from aerosol scattering and absorption measurements, while Ångström exponents were calculated by means of the three wavelengths (450 nm, 525 nm, 635 nm) aerosol light scattering measurements from Nephelometer. Mean scattering and hemispheric backscattering coefficients (@ 635 nm) were $26.8 \pm 23.3\,Mm^{-1}$ and $4.3 \pm 2.7\,Mm^{-1}$, respectively and the mean aerosol absorption coefficient was $2.8 \pm 2.2\,Mm^{-1}$. Mean values of Single Scattering Albedo (SSA) and Ångström exponent (calculated from 450 nm to 635 nm) at MSY were 0.90 ± 0.05 and 1.2 ± 0.6, respectively. A clear relationship was observed between the PM_1/PM_{10} and $PM_{2.5}/PM_{10}$ ratios as a function of the calculated Ångström exponents. Mass scattering cross sections for fine mass and sulfate at 635 nm were calculated in $2.8 \pm 0.5\,m^2\,g^{-1}$ and $11.8 \pm 2.2\,m^2\,g^{-1}$ respectively, while the mean aerosol absorption cross section was estimated around $10.4 \pm 2.0\,m^2\,g^{-1}$. The variability in aerosol optical properties in the WMB were largely explained by the origin and ageing of air masses over the measurement site. The sea breeze played an important role in transporting pollutants from the developed WMB coastlines towards inland rural areas, changing the optical properties of aerosols. Aerosol scattering and backscattering coefficients increased by around 40 % in the afternoon when the sea breeze was fully developed while the absorption coefficient increased by more than 100 % as a consequence of the increase in BC concentration at MSY observed under sea breeze circulation. The analysis of the Ångström (Å) exponent as a function of the origin the air masses revealed that polluted winter anticyclonic conditions and

ACPD

11, 14091–14125, 2011

summer recirculation scenarios typical of the WMB led to an increase of fine particles in the atmosphere (Å = 1.4 ± 0.1) while the aerosol optical properties under Atlantic Advection episodes and Saharan dust outbreaks were clearly dominated by coarser particles (Å = 0.7 ± 0.3).

1 Introduction

The Mediterranean Basin is a very complex area where orography and atmospheric dynamics coupled with a large variety of aerosol sources give rise to a complex mixture of atmospheric particulate matter (PM). Delimited to the north by the European continent and to the south by the North African arid regions, it is largely affected by Saharan dust, marine aerosols, and anthropogenic emissions from both the highly industrialized/urbanized coastline around the Basin and the European continent. Thus, the Mediterranean represents a unique area in terms of suspended particulate matter (Lelieveld et al., 2002; Ichoku et al., 2002). In order to better understand the role of PM on climate in such complex scenarios, the measurements of aerosol optical properties such as aerosol extinction, absorption, and single scattering albedo (SSA) are needed. In fact, the particles in the atmosphere affect the Earth's climate by cooling or heating the atmosphere depending on their scattering and absorbing properties with respect to the solar and terrestrial radiation. However, the magnitude of the current aerosol effect on climate is very poorly defined given that aerosols are present in the atmosphere in a huge variety of sizes, shapes, chemical composition, refractive index, etc. Fine particles with aerodynamic diameter lower than 1 µm (PM_1) are highly effective in scattering and absorbing solar radiation depending on their chemical composition. Particles which have a net cooling effect of the atmosphere and the Earth's surface are sulphate particles which strongly scatter the sun light, while soot particles (or black carbon, BC) have strong absorbing properties over the entire visible spectrum which lead to a warming of the atmosphere. Due to the variety of the regions around the Mediterranean basin, long-term detailed in situ experiments aimed to the

ACPD
11, 14091–14125, 2011

determination of aerosol optical properties are needed. As shown in this work, the in situ measurements are helpful in order to describe the effects of mesoscale weather systems such as the breeze circulation on aerosol optical properties. A number of studies have been published on in situ aerosol optical measurements in the Eastern Mediterranean (Vrekoussis et al., 2005; Ichoku et al., 1999; Formenti et al., 2001; Sciare et al., 2005; Kouvarakis et al., 2002; Andreae et al., 2002; Gerasopoulos et al., 2003; Sabbah et al., 2001; Israelevich et al., 2002), Central Mediterranean and South Italy (Pace et al., 2006; Esposito et al., 2004), South Iberian Peninsula (Pereira et al., 2011; Lyamani et al., 2008). However, little has been published on aerosol optical properties in the Western Mediterranean Basin (Mallet et al., 2003; Saha et al., 2008). As evidenced by a number of publications, the WMB undergoes severe pollution episodes affecting not only the coastal sites closest to the emission sources, but also the more elevated rural and remote areas inland due to thermally driven winds (Querol et al., 2007; Pérez et al., 2008a; Pey et al., 2009, 2010; Salameh et al., 2006; Pandolfi et al., 2011). These studies were mainly dedicated to the study of the chemical composition and physical properties of the atmospheric aerosols.

In this study we report 1 year of simultaneous aerosol optical and chemical properties measured at a regional background site in the WMB. The evolution of aerosol scattering, backscattering and absorption coefficients, Ångström exponent and single scattering albedo are presented and discussed. The relationship of the aerosol optical properties with PM and sulfate concentrations is also discussed. Moreover, the change in aerosol optical properties as a function of both synoptic and meso-to-local transport scenarios is studied.

ACPD
11, 14091–14125, 2011

2 Methodology

2.1 Measurement site

Simultaneous measurements and sampling of PM levels, chemical composition and optical properties were performed during the period November 2009–October 2010 at Montseny (MSY, 41°46′ 45.63″ N 02°21′ 28.92″ E, 720 m a.s.l.) a rural site in NE of Spain (Fig. 1). The MSY site is part of the EUSAAR network (European Supersites for Atmospheric Aerosol Research, www.eusaar.net) recently created to integrate the measurements of atmospheric aerosol properties at 21 European ground-based stations. The MSY station is located within a regional natural park about 50 km to the NNE of the city of Barcelona (BCN) and 25 km from the Mediterranean coast. The selected site represents the typical regional background conditions of the WMB characterized by severe pollution episodes affecting not only the coastal sites closest to the emission sources, but also the more elevated rural and remote areas land inwards due to thermally driven winds (Pérez et al., 2008a; Pey et al., 2010). The effect of these particular atmospheric conditions on the aerosol optical properties is discussed in the following paragraphs.

2.2 Measurements

Particles scattering (σ_{sp}) and hemispheric backscattering (σ_{bsp}) coefficients were measured with a LED-based integrating nephelometer (model Aurora 3000, ECOTECH Pty, Ltd, Knoxfield, Australia). The instrument measures aerosol scattering and backscattering coefficients at 450 nm, 525 nm and 635 nm. A full calibration of the nephelometer was performed three times per year by using CO_2 as span gas while zero measurements and adjusts were performed once per week by using internally filtered particle free air. Scattering measurements from nephelometers need to be corrected for truncation errors due to non-ideal detection of scattered radiation. Thus, the experimental setups of nephelometers limit the collection of radiation scattered around both the

ACPD
11, 14091–14125, 2011

backward (180°) and forward (0°) directions. The Aurora 3000 for example operates by collecting light scattered within the range 10°–170°. A detailed description of the instrument is given by Müller et al. (2010a). Compared to backscatter the main source of error is the truncation in the forward direction (0°–10°) where the radiation scattered by particles increases with increasing particle size (van de Hulst, 1957). Thus, the scattering correction factor ($C_{sp,\lambda}$) is a function of the size of the particles. Moreover, $C_{sp,\lambda}$ also includes another source of error which is the non-ideal (non-Lambertian) illumination function of the light source. Müller et al. (2010a) provided the parameterization needed to calculate $C_{sp,\lambda}$ once the volume median diameter of the particle size distribution is known and compared corrected and non-corrected data from Aurora 3000 to another commercial instrument (TSI model 3563) that was fully described by Anderson et al. (1996) and Anderson and Ogren (1998). Anderson and Ogren (1998) provided a correction factor based on the measured Ångström exponent which is often used for aerosol size characterization. As shown in the next paragraph the Ångström exponents can be easily calculated by means of the multi-wavelength total scattering measurements from nephelometers. After correction, both instruments agreed very well with differences for total scattering between 2 % and 5 % and coefficients of determination (R^2) higher than 0.99 (Müller et al., 2010a). Given that the measurements of the volume median diameter of the particle population was not available, in the present work the data from the Aurora 3000 were corrected by using both the Ångström-based parametrization of Anderson and Ogren (1998) and the experimental comparison provided by Müller et al. (2010a) between Ecotech and TSI nephelometers after correction.

In order to prevent the presence of liquid particles inside the sampling cell a relative humidity (RH) threshold of 60 % was set by using a processor-controlled automatic heater inside the nephelometer. Müller et al. (2010a) measured detection limits of Aurora 3000 over a one minute averaging time at wavelengths 450 nm, 525 nm, and 635nm of 0.20, 0.12, 0.29 Mm^{-1} for total scattering, and 0.06, 0.07, 0.04 Mm^{-1} for backscattering, respectively.

ACPD
11, 14091–14125, 2011

Black carbon (BC) mass concentrations at 637 nm (Müller et al., 2010b) and particle number concentrations during the study period were measured with Multi Angle Absorption Photometers (MAAP, model 5012, Thermo) and a Condensation Particle Counters (CPC), respectively. The detection limit of the MAAP instrument is lower than 100 ng m^{-3} over 2 min integration.

The nephelometer, MAAP and CPC instruments were connected to the same sampling line with the inlet, with a cut-off diameter of 10 µm, placed at about 1.5 m above the roof of the cabin hosting the instruments. In this work the aerosol scattering and backscattering coefficients and BC and particle number concentrations were integrated over 1 h.

Real time PM_{10}, $PM_{2.5}$ and PM_1 concentrations were continuously measured, on an hourly basis, by using a GRIMM optical counter (model 1107). Subsequently, the PM concentrations were corrected with factors obtained by comparing real time and gravimetric measurements. PMx gravimetric measurements on a 24 h basis were performed twice per week with high volume samplers (DIGITEL and MCV at 30 m^3 h^{-1}) with appropriate (PM_1, $PM_{2.5}$, PM_{10}) cut-off inlets. Samples were collected on quartz fibre filters and analysed following the experimental procedures described in Querol et al. (2001) for the concentrations of major (Al, Ca, K, Mg, Fe, Ti, Mn, P, S, Na) and NO_3^-, SO_4^{2-}, NH_4^+ and Cl^- species. In this work the measured concentrations of sulfate were used for comparison with the scattering properties of the aerosols. Levels of elemental carbon (EC) were determined from the collected filters by means of a SUNSET analyzer and subsequently used for the calculation of aerosol absorption cross section as described in the following paragraphs.

Ambient temperature, relative humidity, pressure, precipitation, wind speed and velocity were measured with a meteorological station placed on the roof of the sampling cabin.

ACPD
11, 14091–14125, 2011

2.3 Data processing

Two aerosol optical parameters, the Single Scattering Albedo (SSA) and the Ångström (Å) exponent, were calculated by using the nephelometer and MAAP data. As known the atmospheric particles have a cooling or warming effect on climate depending on the SSA value. Non-absorbing particles such as sulfate have an SSA of one while lower SSA values indicate the presence of more absorbing particles. The SSA at a given wavelength λ is given by:

$$\mathrm{SSA}(\lambda) = \frac{\sigma_{\mathrm{sp}}\ (\lambda)}{\sigma_{\mathrm{sp}}\ (\lambda) + \sigma_{\mathrm{ap}}\ (\lambda)} \tag{1}$$

where $\sigma_{\mathrm{ap}}(\lambda)$ is the particles absorption coefficient at the wavelength λgiven by $\sigma_{\mathrm{ap}}(\lambda)$ $[\mathrm{m}^{-1}] = \mathrm{BC}\ [\mathrm{gm}^{-3}] \times \sigma\ (\lambda)\ [\mathrm{m}^2\mathrm{g}^{-1}]$ (Petzold and Schönlinner, 2004) where $\sigma(\lambda)$ is the absorption cross section. We calculated the hourly SSA values from equation 1 by using the σ_{sp} at 635 nm obtained with the nephelometer and the σ_{ap} at 637 nm taken with the MAAP. Thus, the σ_{ap} was calculated by dividing the equivalent BC concentration given by the MAAP by $6.6\,\mathrm{m}^2\,\mathrm{g}^{-1}$ which is the value of the absorption cross section recommended by the manufacturer. Then, following the experimental procedure described in Fernández-Camacho et al. (2010) and Reche et al. (2011), the actual aerosol absorption cross section $\sigma\ (\lambda)$ was determined by comparing the absorption coefficient $\sigma_{\mathrm{ap}}(\lambda)$ measured by the MAAP with the concentrations of EC in the collected PM_{10} filters as reported in Fig. 2. An average value of $\sigma\ (\lambda) = 10.4 \pm 2.0\,\mathrm{m}^2\,\mathrm{g}^{-1}$ was obtained and used to correct the equivalent concentration of BC given by the MAAP instrument. Absorption cross sections between $8\,\mathrm{m}^2\,\mathrm{g}^{-1}$ and $11\,\mathrm{m}^2\,\mathrm{g}^{-1}$ are usually reported in literature (see for example Fernández-Camacho et al., 2010; He et al., 2009; Barnard et al., 2008; Arnott et al., 2003, 2005).

ACPD
11, 14091–14125, 2011

The second retrieved aerosol optical parameter was the Ångström exponent which describes the λ-dependence of particle scattering coefficient and it is given by:

$$\mathring{A} = -\frac{\log\left(\sigma_{sp}^{\lambda_1} / \sigma_{sp}^{\lambda_2}\right)}{\log\left(\lambda_1 / \lambda_2\right)} \quad (2)$$

An Ångström exponent of 4 represents the scattering from molecules (Rayleigh's regime). Thus, a large Å (higher than 2) implies scattering dominated by submicron particles, while Å values lower than one represent an aerosol distribution dominated by coarser particles.

3 Results

3.1 General features

Figure 3 shows the temporal series of the atmospheric components and aerosol parameters measured at MSY station while means, standard deviations, medians, skewness, percentiles, minimum and maximum values were reported in Table 1. The skewness measures the asymmetry of a distribution function and the higher the skewness, the higher the probability of measuring high levels for the considered aerosol component or parameter. Hourly PM_1 levels at MSY during the study period (November 2009–October 2010) ranged between about 2 $\mu g\,m^{-3}$ and 63 $\mu g\,m^{-3}$ with mean value and standard deviation of $10.1 \pm 7.5\,\mu g\,m^{-3}$. As shown later the lowest PM_1 levels at MSY were measured under Atlantic Advection episodes typically observed during the cold season in the WMB (Pey et al., 2010) and causing the renovation of accumulated pollution in the aged air masses. Conversely, high PM_1 levels were related with both summer regional episodes, characterized by frequent recirculation of air masses and subsequent layering of aerosols over the WMB (Rodríguez et

ACPD
11, 14091–14125, 2011

al., 2003; Pérez et al., 2004), and winter anticyclonic/accumulation episodes leading to the increase of atmospheric pollution around the emission sources. The winter episodes are recurrently coupled with transport of air masses from Central Europe (Pey et al., 2010). As discussed in the following, of this work these two extreme scenarios (the Atlantic advection and pollution episodes) where characterized by particulate matter with different optical properties. During the measurement period the scattering and hemispheric backscattering coefficients (@ 635 nm) ranged between 0.3 Mm^{-1} and 204 Mm^{-1} (mean = 26.8 ± 23.3 Mm^{-1}) and between 0.3 Mm^{-1} and 23 Mm^{-1} (mean = 4.3 ± 2.7 Mm^{-1}), respectively. Hemispheric backscatter measurements were implemented in the used Aurora 3000 nephelometer from the end of May 2010. The aerosol absorption coefficient (@ 635 nm) ranged between about 0.0 Mm^{-1} and 34 Mm^{-1} with a mean value of 2.8 ± 2.2 Mm^{-1}. Mean values of the measured optical properties at 450 nm and 525 nm are reported in Table 1. As reported in literature the aerosol optical properties measured with nephelometers vary substantially depending on the location of the measurement site. Mean values of aerosol absorption and scattering in the visible range of about 60–80 Mm^{-1} and 230–300 Mm^{-1} respectively were registered in large urban areas as Beijing (He et al., 2009) and Mexico City (Silvia, 2002; Paredes-Miranda et al., 2009). Scattering and absorption coefficients with mean values higher than 700 Mm^{-1} and 80 Mm^{-1} respectively were measured in a highly polluted site close to New Delhi (Hyvärinen et al., 2010). In Artic remote sites mean scattering and absorption coefficients lower than 10 Mm^{-1} and 1 Mm^{-1}, respectively were measured (Aaltonen et al., 2006; Delene and Ogren, 2002). At different locations in the Eastern Mediterranean Basin scattering coefficients at 550 nm within the range 50–90 Mm^{-1} and absorption coefficients of about 5–6 Mm^{-1} were registered (Vrekoussis et al., 2005; Gerasopoulos et al., 2003; Andreae et al., 2002). These relatively high values reflected from one side the effect of the Saharan dust events frequently observed in the Mediterranean Basin and from the other side the impact of continental pollution on the Eastern Mediterranean coast. In a continental site anthropogenically influenced by high sulfate burden Delene and Ogren (2002) measured values of the

ACPD
11, 14091–14125, 2011

absorption and scattering coefficients at 550 nm of about 5 Mm^{-1} and 60 Mm^{-1}, respectively. Recently, mean scattering and backscattering coefficients of 42.5 Mm^{-1} and 5.9 Mm^{-1} respectively were measured in a small city quite far from pollution sources in the southwestern Portugal (Pereira et al., 2011). In an urban environment in the South of Spain, scattering and absorption coefficients of 84 Mm^{-1} and 28 Mm^{-1} respectively were measured (Lyamani et al., 2006).

The MSY measurement site can be considered as a regional background site influenced – under specific atmospheric conditions as discussed in the following paragraphs – by emissions from the urbanized/industrialized WMB coastline. Mean values of BC, particle number concentration, SSA and Ångström exponent at MSY during the study period were 281 ± 223 ng m^{-3}, 3682 ± 3241 cm^{-3}, 0.90 ± 0.05 and 1.2 ± 0.6, respectively. The measured mean SSA and Ångström exponent were found to be consistent with those reported by Mallet et al. (2003) and Saha et al. (2008) respectively for South France. The Ångström exponent is often used as a qualitative indicator of aerosol particle size, with values greater than 2 indicating small particles, and values less than 1 indicating large particles like sea salt and dust (Schuster et al., 2006). Figure 4 shows the 24 h averaged Ångström exponents as a function of the PM_1-to-PM_{10} and $PM_{2.5}$-to-PM_{10} ratios. A clear increasing tendency of the PM ratios was observed with increasing Ångström exponents. For a calculated mean Å of 1.2 the PM_1/PM_{10} and $PM_{2.5}/PM_{10}$ ratios were found around 0.6 and 0.8 respectively indicating a higher percentage of small particles in the atmosphere compared with coarse particles. As reported in Pereira et al. (2011) about 60–70 % of the light is scattered by submicron particles for an Ångström exponent of 1.5. As shown in the following of this work, the submicron particles dominated even more the light scattering at MSY under specific atmospheric conditions leading to the presence of polluted air masses at MSY station.

As suggested by Cermac et al. (2010), negative Ångström exponents could be an indication of reduced anthropogenic emissions with prevalence of coarse-mode particles. Negative Ångström exponent and high Aerosol Optical Depth (AOD) have been also observed and related with transport of coarse-mode dust in northern India by

ACPD
11, 14091–14125, 2011

Singh et al. (2004). However, extremely negative values of the Ångström exponents are unfeasible for atmospheric aerosols. Similarly, the Ångström exponent cannot be higher than about 4 which represent the limit given by the Rayleigh regimen for the molecular scattering. In the present case 57 values of the Ångström exponent out of 7834 hourly values were smaller than −1 (0.7 %) and 5 values were higher than 4 (0.06 %). Moreover, Table 1 indicates that the 1-th and the 99th percentiles for the Ångström exponent were −0.7 and 2.1, respectively. Figure 5 shows the distribution of the scattering coefficient at 635 nm as a function of the calculated hourly Ångström exponents. As reported in the Figure both negative and positive Ångström exponents were always related with low scattering coefficients. A closer analysis of the air mass origin revealed the absence of Saharan dust intrusions during negative Å values and the prevalence of Atlantic advection episodes leading to low PM concentrations. The mean PM_{10} and PM_1 concentrations were in fact $4.3 \pm 1.6\,\mu g\,m^{-3}$ and $2.3 \pm 1.2\,\mu g\,m^{-3}$ respectively when measuring negative Å. Over the entire study period the mean PM_{10} concentration was $16.6 \pm 11.9\,\mu g\,m^{-3}$. Consequently, the measured extremely negative and positive Ångström exponents were likely due to instrumental noise under very low scattering conditions. Note also that, as reported in Fig. 4, on a daily basis the Ångström exponents were always positive and smaller than 4. Similar behaviour of the Ångström exponent was also observed in a remote subartic site by Aaltonen et al. (2006). Furthermore, the lowest values for single scattering albedos are about 0.2 for pure black carbon (Virkkula et al., 2005) and SSA cannot be higher than 1 by definition of SSA. The 1-th and the 99-th percentiles for SSA were 0.71 and 0.97, respectively and only 6 hourly values of the SSA out of 6952 (0.09 %) were higher than 1.0. Thus, these extreme SSA values were also related with instrumental noise.

3.2 Mass scattering cross section for fine mass and SO_4^{2-}

The measurements of aerosol scattering coefficients can be used as a surrogate for fine PM concentrations, thus the scattering of light (σ_{sp}) is proportional to the particle

ACPD
11, 14091–14125, 2011

number density and consequently to the mass of particles in the atmosphere. The relationship between particle number density and mass depends on the physical properties of the aerosol such as size, shape, density, etc. Figure 6a shows the correlation between σ_{sp} at 450, 525, and 635 nm and PM_1 concentrations expressed in $\mu g\,m^{-3}$. Very good correlations were observed with coefficients of determination R^2 higher than 0.86. The slopes of the fitting lines represent the fine mass scattering cross sections which ranged between around $2.8 \pm 0.5\,m^2\,g^{-1}$ at 635 nm and $4.4 \pm 0.8\,m^2\,g^{-1}$ at 450 nm. The reduction of the mass scattering cross section with increasing wavelength reflects the $\lambda^{-\text{Å}}$ dependence of σ_{sp}. Despite the good correlations observed in Figure 6a the reported data scattered considerably around the mean given by the fitting lines. This spreading of the data reflects the changes in the microphysical properties of the measured aerosols which can occur over a small time-scale. By including the intercepts when fitting the hourly data of Fig. 6a (not shown) these intercepts assumed very low values around $-3 \div -1\,Mm^{-1}$. Thus, in the hypothetical case of zero PM concentration in the atmosphere also the scattering coefficients approximated, within the errors, to very low values close to the Rayleigh regimen only. Figure 6b shows the relationship between the 24h-averaged σ_{sp} at the three wavelengths and the 24h-average fine (PM_1) sulfate concentrations expressed in $\mu g\,m^{-3}$. A good correlation was observed also for fine sulfate particles with R^2 higher than 0.82 after excluding specific days highlighted by the orange boxed areas. In these specific days the high measured scattering coefficients were likely due to high concentrations of coarse crustal particles ($<C>_{PM10} = 8.5 \pm 12.7\,\mu g\,m^{-3}$) which favoured the absorption of species like SO_2 and the formation of coarse SO_4^{2-} ($<SO_4^{2-}>_{PM10} = 2.0 \pm 0.9\,\mu g\,m^{-3}$) thus increasing the scattering. In fact, the mean $<C>_{PM10}$ and $<SO_4^{2-}>_{PM10}$ calculated over the points included in the fitting process were $1.7 \pm 1.2\,\mu g\,m^{-3}$ and $0.7 \pm 0.5\,\mu g\,m^{-3}$, respectively. The $<C>_{PM10}$ concentrations were calculated as the sum of Al_2O_3, SiO_2, CO_3^{2-}, Ca, Fe, K, Mg, Mn, Ti and P (see Querol et al. (2001) for details) and all the points within the orange boxed areas were collected during the period November 2009–

ACPD
11, 14091–14125, 2011

April 2010. The fitting lines of Figure 6b were calculated by adding the y-intercept which indicated a non-zero scattering of light when fine sulfate concentration was close to zero. Thus, even if dominated by fine sulfate particles, the measured scattering of light was due in part to other atmospheric components than fine sulfate thus leading to the observed positive values of the intercepts. Scattering cross sections for fine sulfate of $11.8 \pm 2.2\,m^2\,g^{-1}$ at 635 nm, $15.6 \pm 2.8\,m^2\,g^{-1}$ at 525 nm, and $20.0 \pm 3.4\,m^2\,g^{-1}$ at 450 nm were calculated (Fig. 6b).

3.3 Correlation between σ_{sp} and aerosol measurements

In this section we studied the relationships between σ_{sp} and measured aerosol components or parameters, such as PM mass, backscattering coefficient (σ_{bsp}), scattering-to-backscattering ratio (*S/B* ratio), absorption coefficient, SSA, Å exponent, BC concentration, and particle number density (Fig. 7). To do this the frequency distribution of hourly σ_{sp} at 635 nm was calculated for values between 0 Mm^{-1} and 130 Mm^{-1} with a bin of 10 Mm^{-1}. Given the low occurrence for σ_{sp} higher than 130 Mm^{-1} (Fig. 5), values higher than 130 Mm^{-1} were excluded in this section. First of all it can be noted the log-normal distribution of σ_{sp} (Fig. 7) showing the typical long tile toward positive high values leading to median values lower than the mean and skewness higher than one (Table 1). The observed distribution of σ_{sp} is typical for many positive defined meteorological parameters (This work, Table 1; O'Neill et al., 2000; Matthias and Bösenberg, 2002; Querol et al., 2009; Pereira et al., 2011). Exceptions from this behaviour in Table 1 was observed for the SSA and the Å exponent showing negative skewness indicating the presence of a tile toward values lowers than the mean in the frequency distributions.

As expected a good correlation was observed between σ_{sp} and PM_1 concentrations (Fig. 7a), these latter also showing low standard deviations. As the σ_{sp} increased, the PM_1 increased monotonically. A similar behaviour was observed for σ_{bsp} and SSA (Fig. 7b and d). If the intensity of light scattering increased, also the aerosol

ACPD
11, 14091–14125, 2011

backscattering of light increased. However, the relative proportion of scattered and backscattered light (Fig. 7c) was not constant being a function of the amount of scattered light. Thus, as the σ_{sp} values increased the *S/B* values were also raised indicating that the total scattering of aerosols increased faster than the backscatter. This observed behaviour was likely due to the increasing importance of the forward scattering ($\theta \sim 0^{\circ}$) compared to backscattering ($\theta \sim 180^{\circ}$) when σ_{sp} increased. Figure 7f shows that the absorbing properties of the aerosols increased as a function of σ_{sp} as a consequence of the observed increase in BC mass concentration in the atmosphere with σ_{sp} (Fig. 7i). Thus, following the relationships reported in the Figs. 6a and 7a for σ_{sp} and PM_1, the concentration of BC is related to the concentration of PM_1. However, the observed increasing tendency of SSA with σ_{sp} (Fig. 7d) suggested that the mean scattering properties of the aerosols for a given volume of sampled air increased faster that the absorption properties for the same volume of air (Fig. 7g). Finally, as reported in Fig. 7h the particle number increased with σ_{sp} as expected from Mie theory (van de Hulst, 1957).

3.4 Diurnal cycles

The diurnal cycles of the considered aerosol components and parameters measured at MSY is reported in Fig. 8. The diurnal cycle of PM_1 concentrations simultaneously measured at an urban background station in Barcelona (the closest big city to MSY station; Fig. 1) is reported for comparison with MSY in order to better interpret the results (Fig. 8a). A detailed description of the Barcelona measuring station is given for example by Pey et al. (2008) and Pérez et al. (2008b). As observed in Figure 8a the levels at MSY during the 24 h were driven by the sea breeze which developed from around 09:00 GMT to 18:00 GMT (Fig. 8e) transporting pollutants from the polluted coastline to the remote areas inland (Pey et al., 2010; Pandolfi et al., 2011). The highest PM_1 concentrations reaching around 12 $\mu g\,m^{-3}$ were measured at MSY under the sea breeze circulation. At the same time the Barcelona monitoring station was cleaned by the sea breeze showing hourly concentrations of PM_1 slightly lower than MSY and

ACPD
11, 14091–14125, 2011

around 11–12 $\mu g\,m^{-3}$ between 13:00 GMT to 17:00 GMT when the sea breeze was fully developed. As reported in Fig. 8e the sea breeze was characterized by an increase in wind velocity which reached 2–3 $m\,s^{-1}$ between 10:00 GMT and 17:00 GMT. As for the PM_1 concentrations, also the aerosol optical properties changed in the late morning-afternoon at MSY. Aerosol scattering and backscattering coefficients increased by around 40 % when the sea breeze was fully developed (13:00–17:00 GMT) if compared with the lower values observed at night-early morning (00:00–08:00 GMT). The scattering coefficient at 635 nm increased from about 22 Mm^{-1} to 34 Mm^{-1} and the backscattering coefficient from 3.7 Mm^{-1} to 5.2 Mm^{-1}. The increase of the absorption coefficient was instead higher and corresponding to about 100 % (from 1.9 Mm^{-1} to 3.9 Mm^{-1}) as a consequence of the strong increase in BC concentrations at MSY observed under sea breeze circulation (~400 $ng\,m^{-3}$, Fig. 8d). Also the particle number concentration increased from values of about 2000–2500 cm^{-3} in the early morning to more than 6000 cm^{-3}. As a consequence of the increase observed in the values of the absorption coefficient the SSA reduced reaching its minimum value of about 0.88 around 13:00 GMT. The Ångström exponent also changes during the day reflecting the increase in the concentration of fine anthropogenic aerosols in the afternoon at MSY. The minimum measured value was around 1.08 at 07:00 GMT and the highest one of about 1.22 at 13:00 GMT. Thus, during the sea breeze circulation the values of the Ångström exponent increased at MSY indicating a higher load of fine particles in the atmosphere during the day compared with night. In Fig. 8c the diurnal cycle of the Ångström exponent calculated from AERONET (the AERosol Robotic NETwork of ground-based sun- and sky-scanning radiometers; see for example Holben et al., 1998) data collected at Barcelona was also reported. The AERONET Ångström exponent was calculated from AOD (aerosol optical depth) data measured at wavelengths of 440 nm and 675 nm and only diurnal data were available. Over the study period the mean value of the Ångström exponent at Barcelona was higher than at MSY with a value of 1.4 ± 0.3 this being consistent with the higher load of fine aerosols expected at urban level compared with the regional level. Moreover, the two reported Ångström

ACPD
11, 14091–14125, 2011

exponent's diurnal cycles in Fig. 8c were clearly anti-correlated with low values measured at Barcelona under sea breeze circulation. The possible explanation for the observed reduction of Ångström exponents at BCN were: (a) the increase of the concentration of coarser marine aerosol in the atmosphere under sea breeze circulation, and b) the cleansing effect of the breeze over the coastline as also demonstrated by the PM_1 diurnal cycle at Barcelona of Fig. 8a. Thus, Fig. 8 gives a picture of the efficiency of the breeze circulations in polluting remote areas in the WMB and shows that the anthropogenic pollution affects both the concentrations and the optical properties of PM.

3.5 Cluster analysis

In order to interpret the variability of PM optical properties as a function of the main different air mass transports, different meteorological tools and aerosol maps were analyzed: back-trajectories of air masses (HYSPLIT4, Draxler and Rolph, 2003); geopotencial height maps (NOAA/ESRL Physical Sciences Division, Boulder Colorado from their Web site at: http://www.cdc.noaa.gov/); aerosol dust concentration maps (BSC/DREAM, NAAPS, and SKIRON); and satellite imagery (NASA-SeaWiFS Project). These tools allowed for the determination of the four main atmospheric scenarios used in this work and affecting the MSY measurement site during the study period. Following the definition given in Pey et al. (2010) these were: (a) Atlantic Advection (AA) episodes (44 days) with air masses coming from the Atlantic Ocean; (b) Winter anticyclonic episodes (WAE) (25 days) causing the stagnation of air masses around the WMB for a few days and subsequent accumulation of pollutants; (c) Saharan dust intrusions (NAF) (13 days); and (d) Regional episodes (REG) (50 days) mainly recorded in summer and characterized by frequent recirculation of air masses over the WMB (Rodríguez et al., 2003; Pérez et al., 2004; Pandolfi et al., 2011). Only clear episodes without precipitations were selected for each category. As reported in Fig. 9 the aerosol components and parameters used in this work show a clear dependence on the origin of air masses. The lowest daily PM_1 levels at MSY were

ACPD
11, 14091–14125, 2011

measured during AA episodes with mean PM_1 concentration of $5.7 \pm 2.8\,\mu g\,m^{-3}$. The effect of the Atlantic Advection episodes was to clean the atmosphere reducing the concentration of fine particles in the atmosphere. Consequently, the σ_{sp}, σ_{bsp} and σ_{ap} reached their minimum values during AA with $14.8 \pm 7.8\,Mm^{-1}$, $2.8 \pm 0.9\,Mm^{-1}$ and $1.8 \pm 1.0\,Mm^{-1}$, respectively. The mean Ångström exponent during AA was 0.7 ± 0.4 indicating the prevalence of coarser particles in the atmosphere and the corresponding reduction of the finest particles. Moreover, while BC concentrations were on average low during AA (BC = 185 ± 100 ng/m^3) the particle number density was high ($4258 \pm 1971\,cm^{-3}$) as a consequence of the enhanced nucleation in the clean atmosphere. The opposite condition was observed under WAE episodes when the highest PM_1 ($19.1 \pm 8.8\,\mu g\,m^{-3}$), σ_{sp} ($55.5 \pm 34\,Mm^{-1}$), σ_{bsp} ($5.7 \pm 1.7\,Mm^{-1}$), σ_{ap} ($5.6 \pm 1.5\,Mm^{-1}$), Ångström exponent (1.4 ± 0.1), BC concentration (581 ± 152 ng/m^3) and number concentration ($4738 \pm 2203\,cm^{-3}$) were measured. The values of σ_{sp} and σ_{bsp} under WAE episodes at MSY were similar to the values registered for example by Pereira et al. (2011) in a small city affected by traffic, indicating the importance of specific atmospheric events in polluting remote/rural areas. Thus, relatively high aerosol scattering and absorption coefficients were attributed to the transport, driven by the breeze, of anthropogenic pollution accumulated for few days over the WMB under WAE scenarios reaching the MSY measurement site (Pandolfi et al., 2011). The presence of polluted air masses at MSY with high levels of fine particles led to the observed high Ångström exponent indicating that a high percentage of light was scattered by submicron particles. A similar result was obtained under the summer REG episodes (Å = 1.4 ± 0.1). The REG episodes were characterized by mean PM concentrations lower than during WAE given the higher dilution of PM in summer and the lack of strong inversions typical of the winter period (Pey et al., 2010; Pandolfi et al., 2011). The NAF episodes were characterized by the transport mainly of coarser particles rather than fine particles with measured PM_1 levels ($10.5 \pm 5.2\,\mu g\,m^{-3}$ at MSY) lying in the typical range of PM_1 levels observed at MSY station (This work; Pey et

ACPD
11, 14091–14125, 2011

al., 2010). As reported in Fig. 9, under AA and NAF episodes the relative proportion of coarser ($PM_{2.5-10}$) particles was higher than during WAE and REG episodes thus leading to the observed lower than 1 Ångström exponent values. A less clear dependence with air mass origin was observed for the SSA, which was on average similar under the reported scenarios. Despite the increase in the absorption coefficient observed under the WAE scenario, the corresponding increase in PM_1 concentration was so high to enhance the mean aerosol scattering properties thus leading to SSA values similar between WAE and AA. Moreover, the absorbing properties of Saharan dust (Vrekoussis et al., 2005) could have accounted, at least in the present case, for the similarity observed between the SSA values during the NAF and WAE episodes.

4 Summary and conclusion

The present work shows how the optical properties of aerosols in rural areas in the Western Mediterranean Basin are highly variable, being dominated not only by the emission sources but also by meteorology. On average, mean values of aerosol scattering, backscattering and absorption coefficients at the regional background station selected for this study (Montseny, NE Spain) were quite low compared with values reported in literature in more industrialized areas or cities around the Mediterranean Basin. However, under specific atmospheric conditions the values of the measured aerosol optical coefficients increased as a consequence of the increase in the concentration of fine particles of anthropogenic origin in the atmosphere. Consequently, also the Single Scattering Albedo (SSA) and the Ångström (Å) exponents calculated in this work changed correspondingly. An interesting feature of all these measured parameters was that these were driven by the sea breeze, which develops in the late morning/afternoon transporting polluted air masses from the highly urbanized/indutrialized coastline toward remote areas inland. Thus, the measured aerosol optical coefficients and the calculated SSA and Å exponents showed a clear diurnal cycle driven by the sea breeze. Moreover, a high level of variability was observed also as a function of the origin of the air masses. Polluted air masses related with both winter and summer regional conditions of stagnation/accumulation over the study area were linked with

ACPD
11, 14091–14125, 2011

an increase in fine particles concentration and an increase in the values of scattering, backscattering and absorption coefficients. On average high Å exponents (around 1.4) were measured under these polluted scenarios as a consequence of the increase in the concentration of fine particles. On the contrary a strong reduction in the Å values (around 0.7) were observed under Atlantic Advection episodes and Saharan dust outbreaks indicating that the optical properties of the aerosols were dominated by the coarse mode. The calculated Ångström exponents were also presented as a function of the fine-to-coarse PM ratios. The result was a clear relationship between PM ratios and Ångström exponent. Thus, high Ångström exponents (>1.2) were clearly related with PM mass dominated by fine particles in the sampled atmosphere.

Acknowledgements. This study was supported by the Ministry of Science and Innovation (CARIATI CGL2008-06294/CLI, GRACCIE CSD2007-00067), the European Union (6th framework CIRCE IP, 036961, EUSAAR RII3-CT-2006-026140). The authors would also like to acknowledge NASA/Goddard Space Flight Center, SeaWIFS-NASA Project, University of Athens, Navy Research Laboratory-USA and the Barcelona Super-Computing Centre for their contribution with TOMS maps, satellite images, SKIRON dust maps, NAAPs aerosol maps, and DREAM dust maps, respectively. The authors gratefully acknowledge the NOAA Air Resources Laboratory (ARL) for the provision of the HYSPLIT transport and dispersion model and/or READY website (http://www.arl.noaa.gov/ready.html) used in this publication. We also thank José M[a]. Baldasano and its staff for theirs effort in establishing and maintaining the Barcelona AERONET measurement site.

References

Aaltonen, V., Lihavainen, H., Kerminen, V.-M., Komppula, M., Hatakka, J., Eneroth, K., Kulmala, M., and Viisanen, Y.: Measurements of optical properties of atmospheric aerosols in Northern Finland, Atmos. Chem. Phys., 6, 1155–1164, doi:10.5194/acp-6-1155-2006, 2006.

Anderson, T. L., Covert, D. S., Marshall, S. F., Laucks, M. L., Charlson, R. J., Waggoner, A. P., Ogren, J. A., Caldow, R., Holm, R. L., Quant, F. R., Sem, G. J., Wiedensohler, A., Ahlquist,

ACPD

11, 14091–14125, 2011

N. A., and Bates, T. S.: Performance characteristics of a high-sensitivity, three wavelength, total scatter/backscatter nephelometer, J. Atmos. Ocean. Tech., 13, 967–986, 1996.
Anderson, T. L. and Ogren, J. A.: Determining Aerosol Radiative Properties Using the TSI 3563 Integrating Nephelometer, Aerosol Sci. Tech., 29, 57–69, 1998.
Andreae, T. W., Andreae, M. O., Ichoku, C., Maenhaut, W., Cafmeyer, J., Karnieli, A., and Orlovsky, L.: Light scattering by dust and anthropogenic aerosol at a remote site in the Negev Desert, Israel, J. Geophys. Res., 107, D2, doi:10.1029/2001JD900252, 2002.
Arnott, W. P., Moosmüller, H., Sheridan, P. J., Ogren, J. A., Raspet, R., Slaton, W. V., Hand, J. L., Kreidenweis, S. M., and Collett Jr., J. L.: Photoacoustic and Filter-Based Ambient Aerosol Light Absorption Measurements: Instrument Comparisons and the Role of Relative Humidity, J. Geophys. Res., 108(D1), 4034, doi:10.1029/2002JD002165, 2003.
Arnott, W. P., Hamasha, K., Moosmüller, H., Sheridan, P. J., and Ogren, J. A.: Towards Aerosol Light Absorption Measurements with a 7-wavelength Aethalometer: Evaluation with a Photoacoustic Instrument and 3 wavelength Nephelometer, Aerosol Sci. Tech., 39, 17–29, 2005.
Barnard, J. C., Volkamer, R., and Kassianov, E. I.: Estimation of the mass absorption cross section of the organic carbon component of aerosols in the Mexico City Metropolitan Area, Atmos. Chem. Phys., 8, 6665–6679, doi:10.5194/acp-8-6665-2008, 2008.
Cermak, J., Wild, M., Knutti, R., Mishchenko, M. I., and Heidinger A. K.: Consistency of global satellite-derived aerosol and cloud data sets with recent brightening observations, Geophys. Res. Lett., 37, L21704, doi:10.1029/2010gl044632, 2010.
Delene, D. J. and Ogren, J. A.: Variability of aerosol optical properties at four North American surface monitoring sites, J. Atmos. Sci., 59, 1135–1149, 2002.
Esposito, F., Leone, L., Pavese, G., Restieri, R., and Serio, C.: Seasonal variation of aerosols properties in South Italy: a study on aerosol optical depths, Ångström turbidity parameters and aerosol size distribution, Atmos. Environ., 38, 1605–1614, 2004.
Fernández-Camacho, R., Rodríguez, S., de la Rosa, J., Snchez de la Campa, A. M., Viana, M., Alastuey, A., and Querol, X.: Ultrafine particle formation in the inland sea breeze airflow in Southwest Europe, Atmos. Chem. Phys., 10, 9615–9630, doi:10.5194/acp-10-9615-2010, 2010.
Formenti, P., Andreae, M. O., Andreae, T. W., Ichoku, C., Schebeske G., Kettle, J., Maenhaut, W., Ptasinsky, J., Karnieli A., and Leliveld, J.: Physical and chemical characteristics of aerosols over the Negev Desert (Israel) during summer 1996, J. Geophys. Res., 106(D5), 4871–4890, 2001.

ACPD
11, 14091–14125, 2011

Gerasopoulos, E., Andreae, M. O., Zerefos, C. S., Andreae, T. W., Balis, D., Formenti, P., Merlet, P., Amiridis, V., and Papastefanou, C.: Climatological aspects of aerosol optical properties in Northern Greece, Atmos. Chem. Phys., 3, 2025–2041, doi:10.5194/acp-3-2025-2003, 2003.

He, X., Li, C. C., Lau, A. K. H., Deng, Z. Z., Mao, J. T., Wang, M. H., and Liu, X. Y.: An intensive study of aerosol optical properties in Beijing urban area, Atmos. Chem. Phys., 9, 8903–8915, doi:10.5194/acp-9-8903-2009, 2009.

Holben, B. N., Eck, T. F., Slutsker, I., Tanré, D., Buis, J. P., Setzer, A., Vermote, E., Reagan, J. A., Kaufman, Y. J., Nakajima, T., Lavenu, F., Jankowiak, I., and Smirnof, A.: AERONET-A federated instrument network and data archive for aerosol characterization, Remote Sens. Environ., 66(1), 1–16, 1998.

Hyvärinen, A.-P., Lihavainen, H., Komppula, M., Panwar, T. S., Sharma, V. P., Hooda, R. K., and Viisanen, Y.: Aerosol measurements at the Gual Pahari EUCAARI station: preliminary 25 results from in situ measurements, Atmos. Chem. Phys., 10, 7241–7252, doi:10.5194/acp-10-7241-2010, 2010.

Ichoku, C., Andreae, M. O., Andreae, T. W., Meixner, F. X., Schebeske, G., Formenti, P., Maenhaut, W., Cafmeyer, J., Ptasisnski, J., Karnieli, A., and Orlovsky, L.: Interrelationships between aerosol characteristics and light scattering during late winter in an eastern Mediterranean arid environment, J. Geophys. Res., 104, 24,371–24,393, doi:10.1029/1999JD900781, 1999.

Ichoku, C., Chu, D. A., Mattoo, S., Kaufman, Y. J., Remer, L. A., Tanre, D., Slutsker, I., and Holben, B. N.: A spatio-temporal approach for global validation and analysis of MODIS aerosol products, Geophys. Res. Lett., 29, 8006, doi:10.1029/2001GL013206, 2002.

Israelevich, P. L., Levin, Z., Joseph, J. H., and Ganor, E.: Desert aerosol transport in the Mediterranean region as inferred from the TOMS aerosol index, J. Geophys. Res., 107(D21), 4572, doi:10.1029/2001JD002011, 2002.

Kouvarakis, G., Doukelis, Y., Mihalopoulos, N., Rapsomanikis, S., Sciare, J., and Blumthaler, M.: Chemical, physical, and optical characterization of aerosols during PAUR II experiment, J. Geophys. Res., 107(D18), 8141, doi:10.1029/2000jd000291, 2002.

Lelieveld, J., Berresheim, H., Borrmann, S., Crutzen, P. J., Dentener, F. J., Fischer, H., Feichter, J., Flatau, P. J., Heland, J., Holzinger, R., Korrmann, R., Lawrence, M. G., Levin, Z., Markowicz, K. M., Mihalopoulos, N., Minikin, A., Ramanathan, V., de Reus, M., Roelofs, G. J., Scheeren, H. A., Sciare, J., Schlager, H., Schultz, M., Siegmund, P., Steil, B., Stephanoul, E. G., Stier, P., Traub, M., Warneke, C., Williams, J., and Ziereis, H: Global air pollution

ACPD
11, 14091–14125, 2011

crossroads over the Mediterranean, Science, 298, 794–799, 2002.
Lyamani, H., Olmo, F. J., and Alados-Arboledas L.: Light scattering and absorption properties of aerosol particles in the urban environment of Granada, Spain, Atmos. Environ., 42, 2630–2642, 2008.
Matthias, V. and Bösenberg, J.: Aerosol climatology for the planetary boundary layer derived from regular lidar measurements, Atmos. Res., 63, 221–245, 2002.
Mallet, M., Roger, J. C., Despiau, S., Dubovik, O., and Putaud, J. P.: Microphysical and optical properties of aerosol particles in urban zone during ESCOMPTE, Atmos. Res., 69, 73–97, 2003.
Müller, T., Laborde, M., Kassell, G., and Wiedensohler, A.: Design and performance of a three-wavelength LED-based total scatter and backscatter integrating nephelometer, Atmos. Meas. Tech. Discuss., 3, 4835–4864, doi:10.5194/amtd-3-4835-2010, 2010.
Müller, T., Henzing, J. S., de Leeuw, G., Wiedensohler, A., Alastuey, A., Angelov, H., Bizjak, M., Collaud Coen, M., Engström, J. E., Gruening, C., Hillamo, R., Hoffer, A., Imre, K., Ivanow, P., Jennings, G., Sun, J. Y., Kalivitis, N., Karlsson, H., Komppula, M., Laj, P., Li, S.-M., Lunder, C., Marinoni, A., Martins dos Santos, S., Moerman, M., Nowak, A., Ogren, J. A., Petzold, A., Pichon, J. M., Rodriquez, S., Sharma, S., Sheridan, P. J., Teinil, K., Tuch, T., Viana, M., Virkkula, A., Weingartner, E., Wilhelm, R., and Wang, Y. Q.: Characterization and intercomparison of aerosol absorption photometers: result of two intercomparison workshops, Atmos. Meas. Tech., 4, 245–268, doi:10.5194/amt-4-245-2011, 2011.
O'Neill, N. T., Ignatov, A., Holben, B. N., and Eck, T. F.: The lognormal distribution as a reference for reporting aerosol optical depth statistics; empirical tests using multi-year, multi-site AERONET sunphotometer data, Geophys. Res. Lett., 27(20), 3333–3336, 2000.
Pace, G., di Sarra, A., Meloni, D., Piacentino, S., and Chamard, P.: Aerosol optical properties at Lampedusa (Central Mediterranean). 1. Influence of transport and identification of different aerosol types, Atmos. Chem. Phys., 6, 697–713, doi:10.5194/acp-6-697-2006, 2006.
Pandolfi, M., Querol, X., Alastuey, A., Jimenez, J., Jorba, O., Stohl, A., Comerón, A., Sicard, M., Pey, J, vanDrooge, B. and the DAURE team: Source and origin of PM in the Western Mediterranean Basin: An Overview of the DAURE campaign, in preparation, Atmos. Chem. Phys. Discuss, 2011.
Paredes-Miranda, G., Arnott, W. P., Jimenez, J. L., Aiken, A. C., Gaffney, J. S., and Marley, N. A.: Primary and secondary contributions to aerosol light scattering and absorption in México City during the MILAGRO 2006 campaign, Atmos. Chem. Phys. 9, 3721–3730, 2009.

ACPD
11, 14091–14125, 2011

Pereira, S. N., Wagner, F., and Silva, A. M.: Seven years of measurements of aerosol scattering properties, near the surface, in the southwestern Iberia Peninsula, Atmos. Chem. Phys. Discuss., 10, 13723–13754, doi:10.5194/acpd-10-13723-2010, 2010.

Pérez, C., Sicard, M., Jorba, O., Comeron, A., and Baldasano, J. M.: Summertime recirculations of air pollutants over the North-Eastern Iberian coast observed from systematic EARLINET lidar measurements in Barcelona, Atmos. Environ., 38, 3983–4000, 2004.

Pérez, N., Pey, J., Castillo, S., Viana, M., Alastuey, A., and Querol X.: Interpretation of the variability of levels of regional background aerosols in the Western Mediterranean, Science of Total Environment, 407, 527–540, 2008a.

Pérez, N., Pey, J., Querol, X., Alastuey, A., Lopez, J. M., Viana, M.: Partitioning of major and trace components in PM_{10}–$PM_{2.5}$–PM_1 at an urban site in Southern Europe, Atmos. Environ., 42, 1677–1691, 2008b.

Petzold, A. and Schönlinner, M.: Multi-angle absorption photometry – a new method for the measurement of aerosol light absorption and atmospheric black carbon, J. Aerosol Sci., 35, 421–441, 2004.

Pey, J., Rodríguez, S., Querol, X., Alastuey, A., Moreno, T., Putaud, J.P. and Van Dingenen, R.: Variations of urban aerosols in the western Mediterranean, Atmos. Environ., 42, 9052–9062, 2008.

Pey, J., Pérez, N., Castillo, S., Viana, M., Moreno, T., Pandolfi, M., Lpez-Sebastián, J.M., Alastuey, A., and Querol, X.: Geochemistry of regional background aerosols in the Western Mediterranean, Atmos. Res., 94, 422–435, 2009.

Pey, J., Pérez, N., Querol, X., Alastuey, A., Cusack, M., and Reche, C.: Intense winter atmospheric pollution episodes affecting the Western Mediterranean, Sci. Total Environ., 408, 1951–1959, 2010.

Querol, X., Alastuey, A., Rodríguez, S., Plana, F., Mantilla, E., Ruiz, C. R.: Monitoring of PM_{10} and $PM_{2.5}$ around primary particulate anthropogenic emission sources, Atmos. Environ., 35, 845–858, 2001.

Pey, J., Pérez, N., Castillo, S., Viana, M., Moreno, T., Pandolfi, M., López-Sebastián, J. M., Alastuey, A., and Querol, X.: Source origin of trace elements in PM from regional background, urban and industrial sites of Spain, Atmos. Environ., 41, 7219–7231, 2007.

Querol, X., Pey, J., Pandolfi, M., Alastuey, A., Cusack, M., Pérez, N., Moreno, T., Viana, M., Mihalopoulos, N., Kallos, G., Kleanthous, S.: African dust contributions to mean ambient PM10 mass-levels across the Mediterranean Basin, Atmos. Environ., 43, 4266–4277, 2009.

ACPD
11, 14091–14125, 2011

Reche, C., Querol, X., Alastuey, A., Viana, M., Pey, J., Moreno, T., Rodríguez, S., González, Y., Fernández-Camacho, R., Sánchez de la Campa, A. M., de la Rosa, J., Dall'Osto, M., Prévôt, A. S. H., Hueglin, C., Harrison, R. M., and Quincey, P.: Variability of levels of PM, black carbon and particle number concentration in selected European cities, Atmos. Chem. Phys. Discuss., 11, 8665–8717, doi:10.5194/acpd-11-8665-2011, 2011.

Sabbah, I., Ichoku, C., Kaufman, Y. J., and Remer, L.: Full year cycle of desert dust spectral optical thickness and precipitable water vapor over Alexandria, Egypt, J. Geophys. Res., 106, 18,305–18,316, 2001.

Saha, A., Mallet, M., Roger, J. C., Dubuisson, P., Piazzola, J., and Despiau, S.: One yearmeasurements of aerosol optical properties over an urban coastal site: Effect on local direct radiative forcing, Atmos. Res., 90, 195–202, 2008.

Salameh, T., Drobinski, P., Menut, L., Bessagnet, B., Flamant, C., Hodzic, A., and Vautard, R.: Aerosol distribution over the western Mediterranean basin during a Tramontane/Mistral event, Atmos. Chem. Phys. Discuss., 6, 11913–11956, doi:10.5194/acpd-6-11913-2006, 2006.

Schuster, G. L., Dubovik, O., and Holben, B. N.: Ångström exponent and bimodal aerosol size distributions, J. Geophys. Res., 111, D07207, doi:101029/2005JD006328, 2006.

Sciare, J., Oikonomou, K., Cachier, H., Mihalopoulos, N., Andreae, M. O., Maenhaut, W., and Sarda-Esève, R.: Aerosol mass closure and reconstruction of the light scattering coefficient over the Eastern Mediterranean Sea during the MINOS campaign, Atmos. Chem. Phys. Discuss., 5, 2427–2461, doi:10.5194/acpd-5-2427-2005, 2005.

Silvia, E. D.: Aerosol impacts on visible light extinction in the atmosphere of Mexico City, Sci. Total Environ., 287, 213–220, 2002.

Singh, R. P., Dey, S., Tripathi, S. N., Tare V., and Holben, B. N.: Variability of aerosol parameters over Kanpur city, northern India, J. Geophys. Res. 109, D23206, doi:10.1029/2004JD004966, 2004.

van de Hulst, H. C.: Light Scattering by Small Particles, Wiley, NY, 1957.

Virkkula, A., Ahlquist, N. C., Covert, D. S., Arnott, W. P., Sheridan, P. J., Quinn, P. K., and Coffman, D. J.: Modification, Calibration and a Field Test of an Instrument for Measuring Light Absorption by Particles, Aerosol Sci. Tech., 39, 68–83, 2005.

Vrekoussis, M., Liakakou, E., Koçak, M., Kubilay, N., Oikonomou, K., Sciare, J., and Mihalopoulos, N.: Seasonal variability of optical properties of aerosols in the eastern Mediterranean, Atmos. Environ., 39, 7083–7094, 2005.

ACPD
11, 14091–14125, 2011

Table 1. Statistics of the considered aerosol components and parameters for the period November 2009–October 2010 at Montseny site. The wavelength (λ) is given in [nm]; Scattering (σ_{sp}), backscattering (σ_{bsp}) and absorption coefficients (σ_{ap}) are given in [Mm^{-1}]; Scattering-to-backscattering ratio (*S/B*), single scattering albedo (SSA) and Ångstrom exponent (Å) are dimensionless; Black carbon (BC) and PM_1 are given in [$\mu g\,m^{-3}$], and particle number (#) is given in [cm^{-3}].

Hourly base	λ	Counts	Mean	SD	Median (50-th perc.)	Min	Max	Skewness	Percentiles 1	10	25	75	99
σ_{sp}	450	7924	40.9	36.2	30.6	0.3	322.3	1.80	1.7	6.6	14.0	57.6	157.8
	525	7924	34.1	30.1	25.5	0.3	270.4	1.88	2.0	5.9	12.1	47.7	134.3
	635	7924	26.8	23.3	20.2	0.3	204.1	1.87	1.9	4.7	9.8	37.5	106.6
σ_{bsp}	450	3989	5.7	3.4	5.3	0.2	28.2	0.85	0.8	1.6	2.9	7.8	15.0
	525	3981	4.9	3.0	4.5	0.3	26.5	0.91	0.5	1.2	2.4	6.7	12.9
	635	3919	4.3	2.7	4.0	0.3	22.8	0.81	0.4	1.1	2.2	6.0	11.4
S/B	450	3989	7.7	1.4	7.8	1.0	18.9	1.82	4.0	6.0	7.0	8.6	10.8
	525	3978	7.6	1.3	7.5	1.3	26.1	2.04	5.0	6.2	6.8	8.2	11.2
	635	3916	7.0	1.3	6.9	1.3	21.0	1.75	4.7	5.7	6.2	7.6	11.3
σ_{ap}	635	7656	2.8	2.2	2.2	0.0	34.3	2.26	0.1	0.6	1.1	3.8	10.3
SSA	635	6952	0.90	0.05	0.91	0.39	1.03	−2.67	0.71	0.85	0.88	0.93	0.97
Å	450–635	7834	1.2	0.6	1.3	−3.9	5.1	−2.12	−0.7	0.47	0.97	1.4	2.1
BC	670	7672	0.271	0.215	0.210	0.005	3294	2.25	0.011	0.053	0.103	0.361	1.052
PM_1	–	8110	10.1	7.5	8.5	0.0	63	1.34	0.5	2.2	4.4	14.3	31.9
#	–	5922	3682	3241	2754	11	34 192	2.59	249	954	1636	4614	15 469

ACPD
11, 14091–14125, 2011

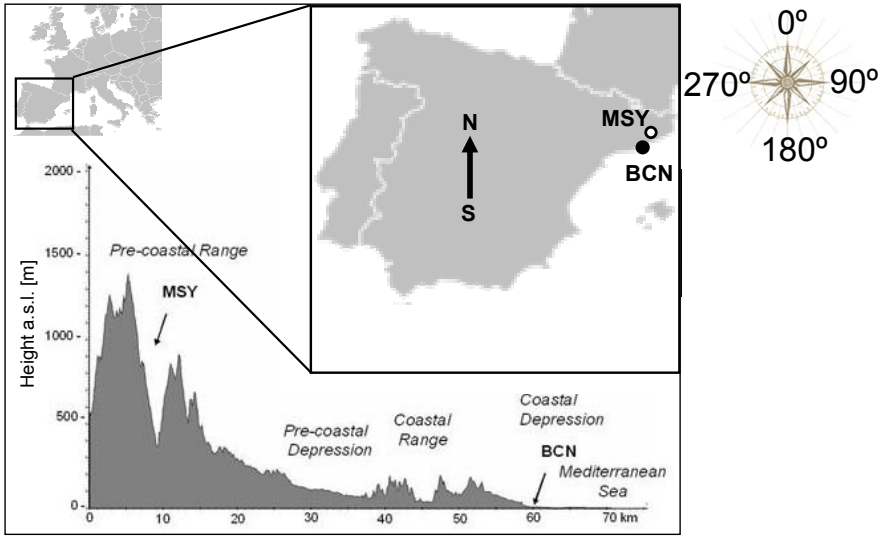

Fig. 1. Location of the Montseny measurement station.

ACPD
11, 14091–14125, 2011

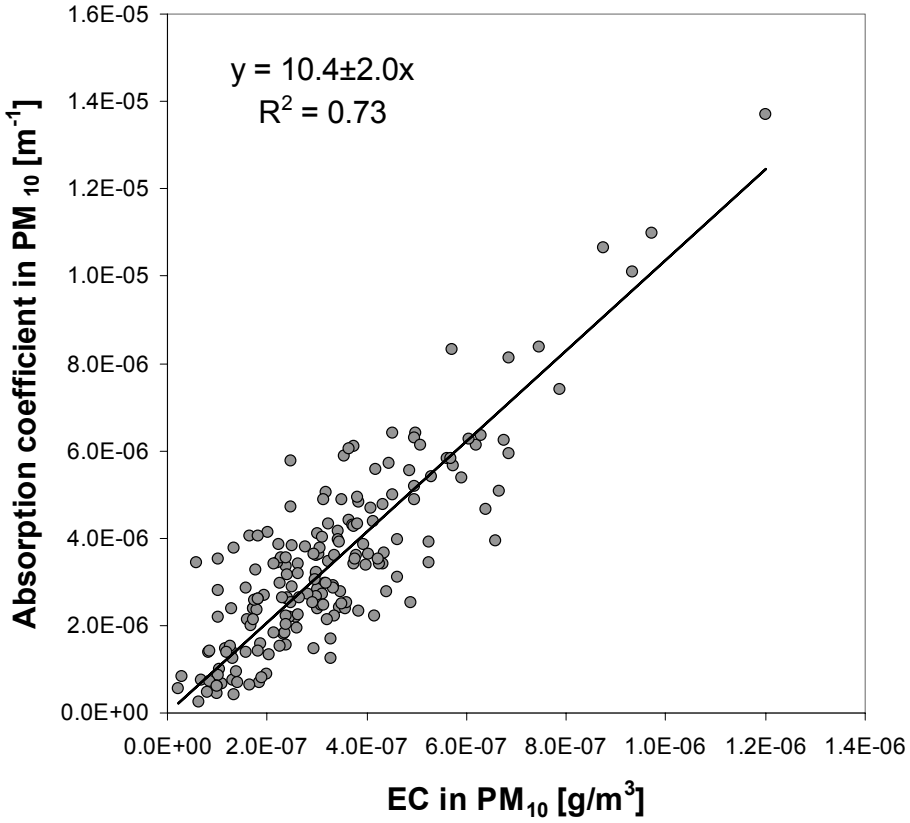

Fig. 2. Correlation between Absorption coefficient from MAAP and 24 h off-line elemental carbon (EC) concentrations from PM_{10} filters.

ACPD
11, 14091–14125, 2011

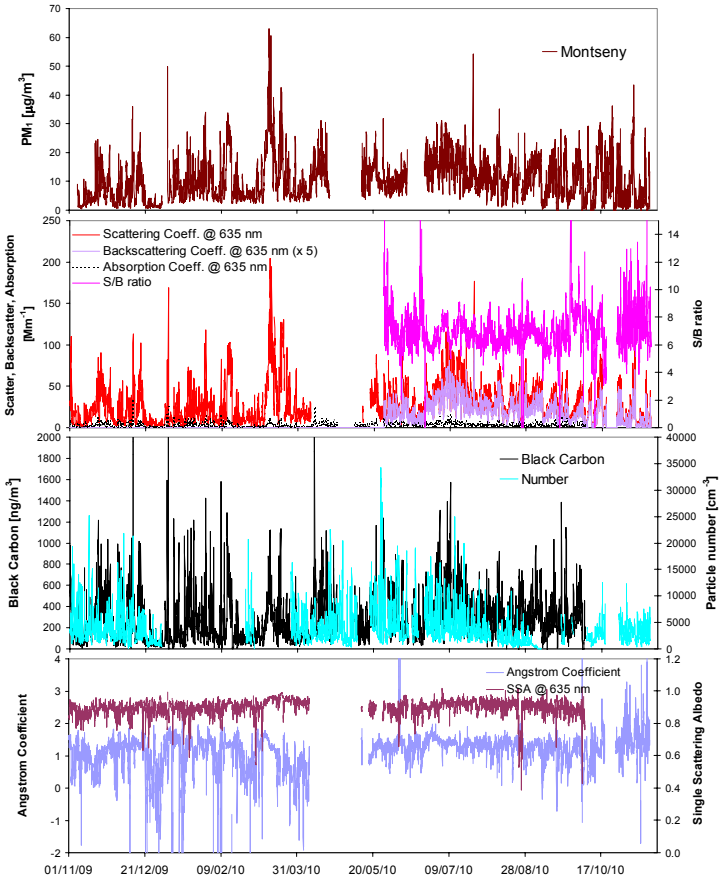

Fig. 3. Temporal series of PM_1 concentrations, scattering coefficient (635 nm), hemispheric backscattering coefficient (635 nm), absorption coefficient (635 nm), scattering-to-backscattering ratio (*S/B*), black carbon concentrations, particle number, Ångström exponent, and Single Scattering Albedo (SSA) at 635 nm.

ACPD
11, 14091–14125, 2011

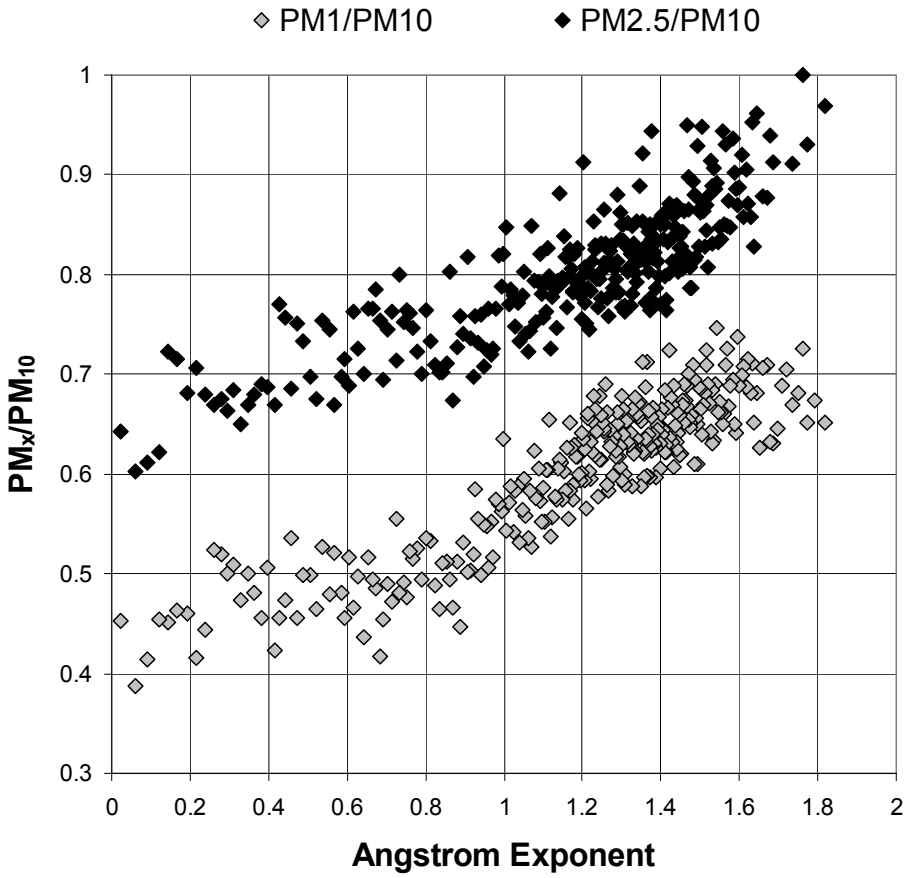

Fig. 4. Correlation between PM_1/PM_{10} and $PM_{2.5}/PM_{10}$ and Ångström exponent.

ACPD
11, 14091–14125, 2011

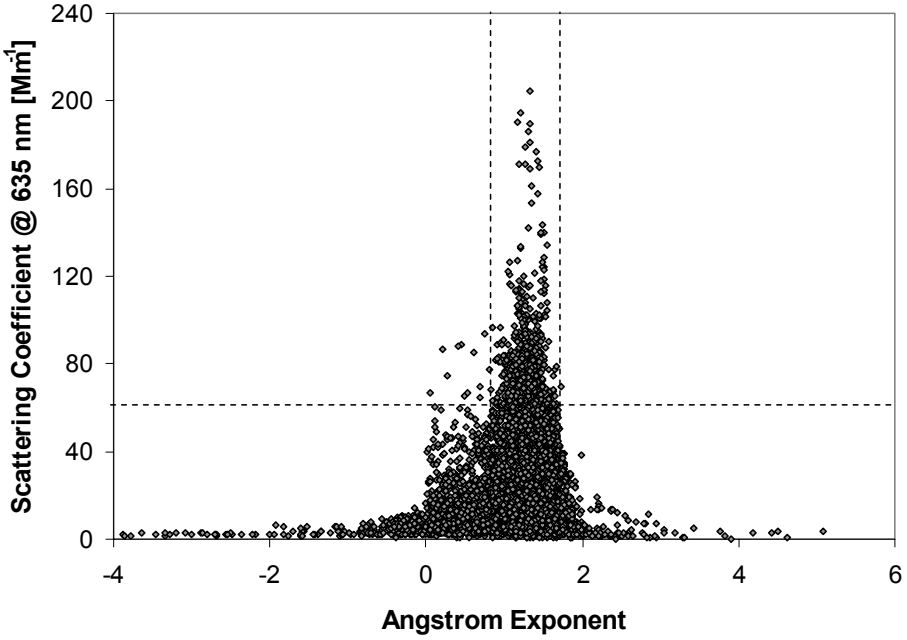

Fig. 5. Scattering coefficient distribution at 635 nm as a function of the Ångström exponent values.

ACPD
11, 14091–14125, 2011

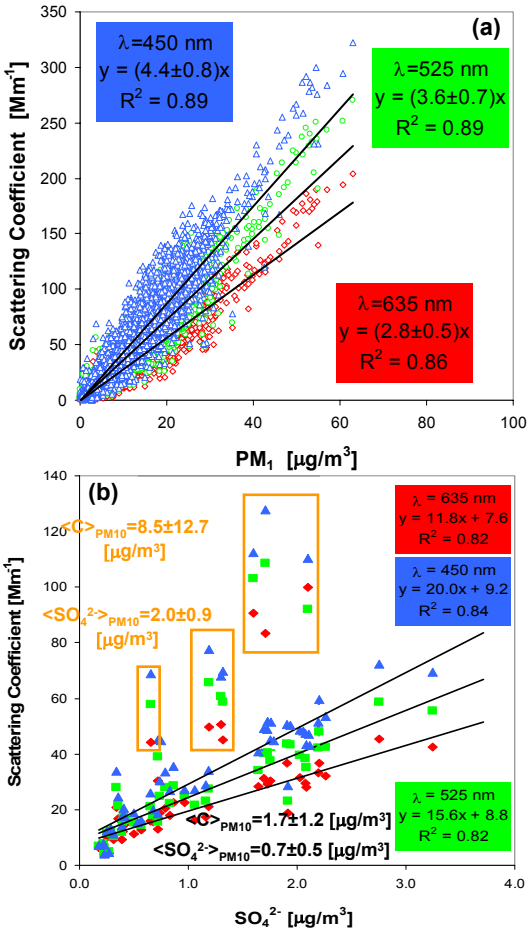

Fig. 6. Correlation between the aerosol scattering coefficients at 450, 525, 635 nm and PM_1 and fine sulfate concentrations.

ACPD
11, 14091–14125, 2011

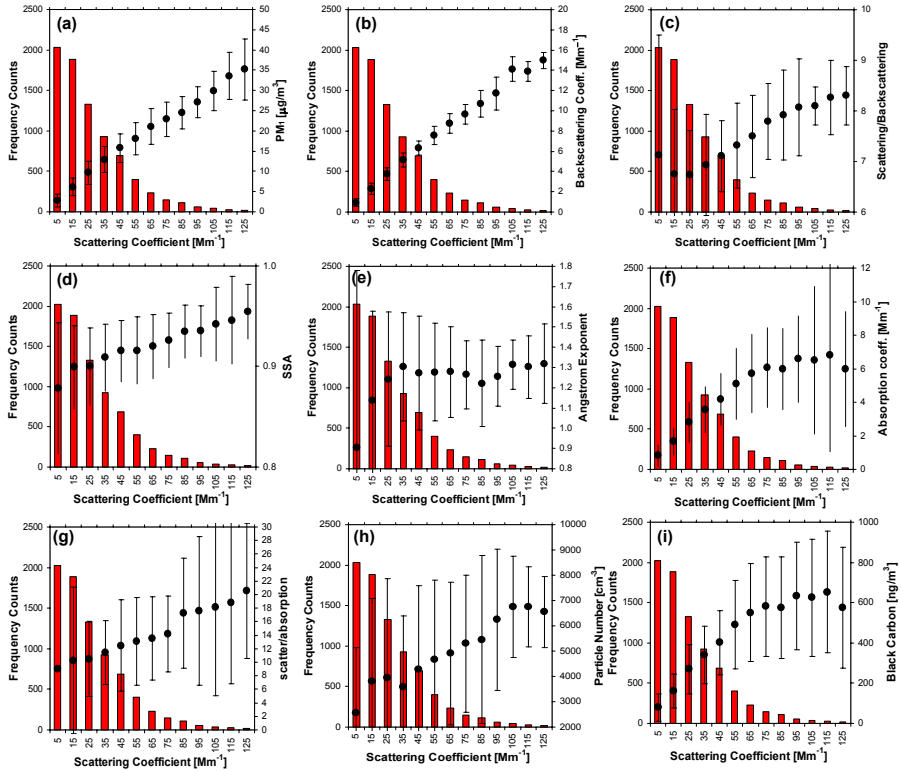

Fig. 7. Correlation between the frequency distribution of aerosol scattering coefficients at 635 nm and **(a)** PM_1 concentration, **(b)** backscattering coefficient, **(c)** scattering-to-backscattering (*S/B*) ratio, **(d)** Single Scattering Albedo, **(e)** Ångström exponent, **(f)** absorption coefficient, **(g)** scattering-to-absorption ratio, **(h)** particle number concentration, and **(i)** black carbon concentrations.

ACPD
11, 14091–14125, 2011

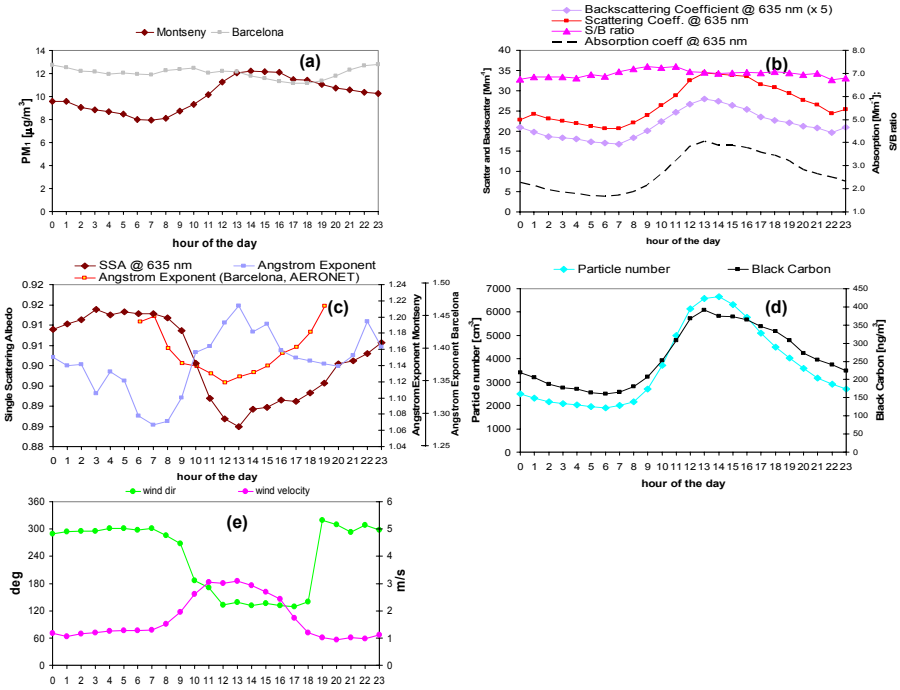

Fig. 8. Diurnal cycles for: **(a)** PM_1 (Montseny and Barcelona), **(b)** scattering coefficient (635 nm), hemispheric backscattering coefficient (635 nm), absorption coefficient (635 nm), scattering-to-backscattering ratio (*S/B*), **(c)** Ångström exponent and Single Scattering Albedo (SSA) at 635 nm at Montseny and Ångström exponent from AERONET data at Barcelona (red line); **(d)** black carbon and particle number concentrations, and **(d)** wind speed and velocity.

ACPD
11, 14091–14125, 2011

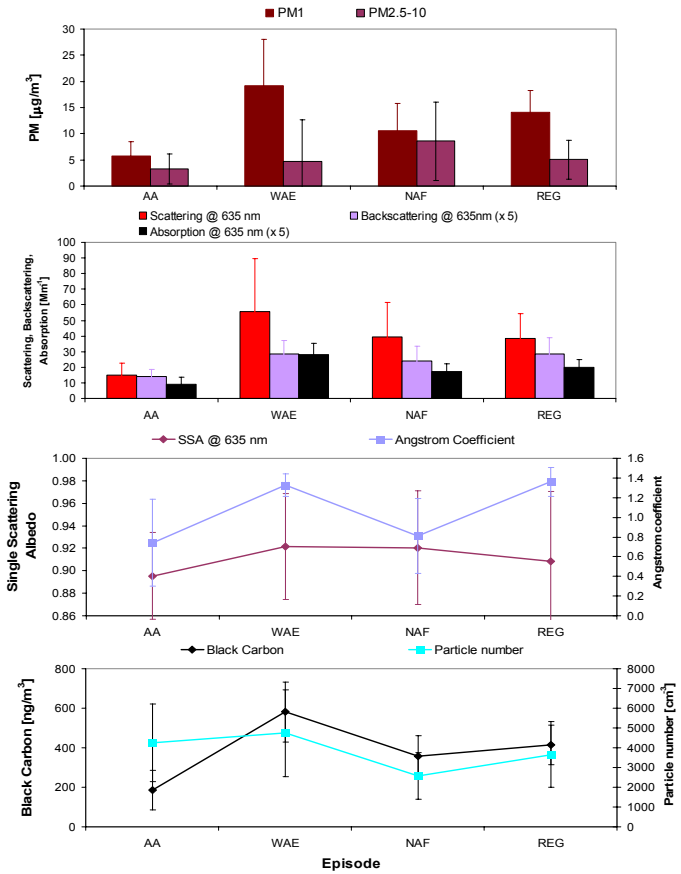

Fig. 9. Aerosol components and parameters as a function of air mass origin: AA = Atlantic Advection; WAE = Winter Anticyclonic Episode; NAF: Saharan dust outbreaks; REG = Regional stagnation episodes.

ACPD
11, 14091–14125, 2011